Medical Oncology (2025) 42:354
https://doi.org/10.1007/s12032-025-02927-7

ORIGINAL PAPER

A novel naphthoquinone compound triggers DNA damage-induced apoptosis on cholangiocarcinoma through upregulation of *BAX*

Gizem Bulut[1,2] · Merve Kayis[3] · Dilan Gezer[4] · Zeliha Gokmen[4] · Zelal Adiguzel[3] · Chiara Raggi[5] · Engin Ulukaya[1,6]

Received: 7 April 2025 / Accepted: 10 July 2025 / Published online: 20 July 2025

Abstract

Cholangiocarcinoma (CCA), a devastating malignancy originating from the bile ducts, is of significant clinical importance due to its rising incidence and poor prognosis. Quinones as being naturally occurring compounds and their frequent utility in anticancer drug development studies seem to be potential sources for the discovery of new chemotherapeutics. In this study, a synthetic naphthoquinone derivative newly synthesized and previously published by our group, named as MK13, has been tested against intrahepatic-CCA (iCCA) cell lines (CCLP1 and HUCCT1). Cell viability was measured with the MTT assay at the doses of 1.56–50 µM for 48 h treatment. Cell death was showed both morphologically with fluorescent double staining and biochemically with flow cytometry analysis of phosphatidylserine translocation. Oxidative stress and DNA damage were also measured with flow cytometry and gene expressions were interpreted via qPCR analysis. MK13 resulted in a strong reduction (about 80%) in viability, especially against CCLP1 cells when compared with doxorubicin. Cell death resulted from apoptosis was shown to be triggered by severe DNA damage that is independent of oxidative stress. Apoptosis was confirmed at molecular level with the upregulation of *BAX*, a pro-apoptotic BH-3 only protein, and *DR5*, a cell surface death receptor. MK13 seems to be a promising anticancer compound against iCCA and deserves further attention for in vivo proof-of-concept studies.

Graphical abstract

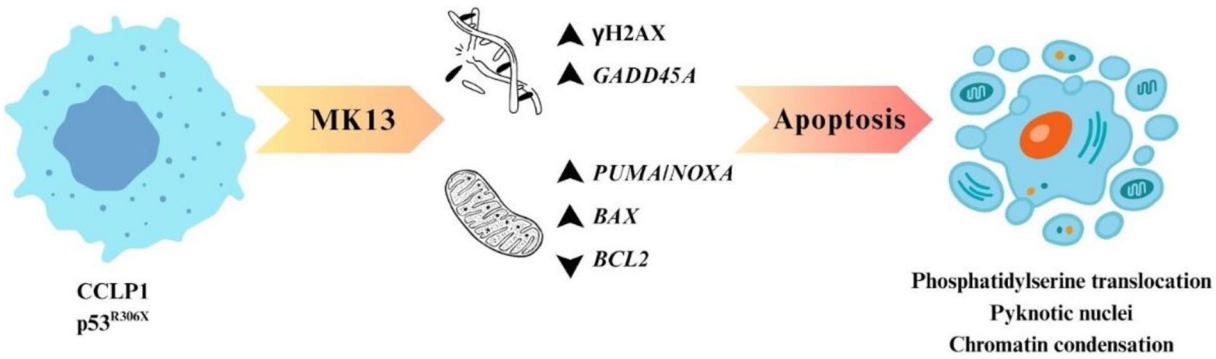

Keywords Anticancer drug · Bile duct cancer · Chemotherapy · Cell death · Quinones

Introduction

Cholangiocarcinoma (CCA) is a malignant tumor originating from the epithelial cells of the bile ducts. It is a highly aggressive adenocarcinoma of the hepatobiliary system and represents the second most prevalent primary liver cancer, accounting for approximately 15% of primary liver malignancies worldwide [1, 2]. CCA is classified into three primary anatomical types: intrahepatic-(iCCA), perihilar, and distal forms—collectively known as extrahepatic CCA (eCCA). Intrahepatic-CCA arises within the liver, perihilar CCA occurs at the hepatic hilum where the bile ducts exit the liver, and distal CCA develops outside the liver [3].

Extended author information available on the last page of the article

This classification holds clinical significance, as it directly influences diagnostic approaches, treatment strategies, and patient outcomes.

Epidemiological studies indicate that the global incidence and mortality rates of CCA, particularly iCCA, are steadily increasing, underscoring the growing clinical burden of this malignancy [4–6]. iCCA is frequently diagnosed at advanced stages, which limits treatment options and contributes to its poor prognosis. When compared with many other malignancies, iCCA exhibits significantly lower survival rates. Although median survival varies by subtype and disease stage, most patients experience an overall survival of less than two years, primarily due to delayed diagnosis [7–9]. In fact, five-year survival rates rarely exceed 30 % in most cases [10].

Current treatment options for CCA include surgical resection, chemotherapy, and radiotherapy. Surgery remains the only potentially curative intervention; however, due to late-stage diagnosis, fewer than 30% of patients present with resectable tumors [11]. As a result, surgery is often not feasible and, even when performed, is associated with high recurrence rates [12]. For patients with unresectable tumors, chemotherapy remains the primary treatment strategy and may help delay disease progression. Commonly used agents include gemcitabine, cisplatin, oxaliplatin, and 5-fluorouracil, with the gemcitabine–cisplatin combination being the most widely adopted regimen. However, the clinical efficacy of these treatments is limited, and overall survival rarely exceeds 1 year [13]. In addition, these therapies are frequently associated with significant adverse effects, including nausea, fatigue, and myelosuppression. Despite their routine use, current chemotherapeutic options are insufficient to achieve meaningful long-term outcomes, underscoring the urgent need for more effective and targeted therapeutic approaches [14]. The absence of reliable early diagnostic markers and a lack of molecularly tailored therapies further highlight the necessity for innovative research to improve outcomes in CCA. These challenges collectively underscore the urgent need for novel, mechanism-based therapeutic strategies.

In response to the limited success of conventional therapies in treating CCA, there is growing interest in identifying novel therapeutic compounds that can selectively target tumor cells and overcome resistance mechanisms. Naturally occurring bioactive molecules have gained attention in this context due to their structural diversity and pharmacological potential. Among them, naphthoquinones (NQs) stand out as a particularly promising class of compounds for anticancer drug development. NQs are a diverse group of molecules characterized by a naphthalene ring bearing two adjacent carbonyl groups. These secondary metabolites are found in a wide range of natural sources, including plants, fungi, and bacteria, where they often serve protective functions in host defense [15]. Their fused aromatic core and redox-active carbonyl moieties confer significant chemical reactivity and contribute to a broad spectrum of biological effects. Although traditionally used in herbal medicine, NQs have gained renewed interest in modern biomedical research, particularly in the field of oncology [16]. In cancer research, NQs have attracted attention for their ability to disrupt essential cellular processes. Several quinone-based agents—such as Adriamycin (doxorubicin), Mitomycin C, and Daunomycin—are already used in clinical oncology. These compounds exert their antitumor effects through mechanisms such as oxidative stress induction, inhibition of topoisomerase II, and activation of apoptotic pathways [17–19]. These multifaceted actions impair cancer cell proliferation and survival, positioning NQs as compelling candidates for targeted cancer therapies. Previous studies by our research group have also explored the anticancer activity of various synthetic NQ derivatives, further reinforcing their therapeutic relevance [20, 21].

Recent literature highlights the growing interest in NQs and related quinone derivatives as potential treatments for CCA. Several studies have shown that these compounds, many of which are naturally derived, can inhibit cancer cell proliferation, induce apoptosis, and modulate key signaling pathways involved in tumor progression and resistance. For example, plumbagin, a plant-derived NQ, has demonstrated efficacy in preclinical CCA models by targeting critical molecular pathways [22]. Similarly, rhinacanthin-C, a natural product isolated from Rhinacanthus nasutus, significantly inhibited proliferation, migration, and invasion through suppression of MAPK signaling and NF-κB activity, and downregulation of MMP-2 expression [23]. Hypocrellin A, a fungal perylenequinone, exhibited potent cytotoxic effects by concurrently modulating the PI3K-AKT-mTOR, MAPK, and STAT3 pathways, reflecting a multitargeted mechanism of action [24]. Thymoquinone, a bioactive constituent of Nigella sativa, induced mitochondrial dysfunction, G2/M cell cycle arrest, and apoptosis, along with a reduction in mitochondrial membrane potential and cytochrome c release [25, 26]. In another study, a naturally occurring anthraquinone derivative shikonin reduced cell viability and induced apoptosis by upregulating caspase-3 and caspase-8, further supporting the relevance of this compound class as anticancer agents [27]. Together, these findings emphasize the therapeutic potential of natural quinone-based molecules in CCA by targeting multiple oncogenic pathways and disrupting mechanisms essential for cancer cell survival. As conventional treatment options continue to offer limited clinical benefit, these compounds represent promising candidates for the development of more effective and targeted therapies.

Building on the promising potential of naturally occurring NQs, recent efforts have focused on developing synthetic derivatives with improved anticancer properties. Our

research group has previously reported the synthesis and structural characterization of several 1,4-naphthoquinone-based compounds, including MK13, which was obtained via a nucleophilic displacement reaction [28–30]. Although earlier studies established the chemical properties and potential anticancer activity of MK13, its biological activity had not yet been explored in the context of CCA. In this study, we investigated for the first time the anticancer effects of MK13 on iCCA cells, with a focus on elucidating its mechanism of action. Our findings reveal that MK13 induces apoptosis through DNA damage in a ROS-independent manner, highlighting its potential as a promising candidate for further preclinical development.

Materials and methods

Cell culture

Human intrahepatic-cholangiocarcinoma (iCCA) cell lines HUCCT1 and CCLP1 were cultured with RPMI 1640 medium (Gibco, USA) supplemented with 10% fetal bovine serum (Gibco, USA) and 1% penicillin–streptomycin. Cells were incubated at 37 °C and 5 % CO_2 condition. When they reached 80% confluency cells were collected with 0.5% trypsin–EDTA (Gibco, USA) for subculturing and seeding. These cell lines were authenticated with STR profiling.

Cytotoxicity and growth rate measurements

Cells were seeded into 96-well culture plates at a density of 5×10^3 cells per well and incubated overnight to allow attachment. The following day, cells were treated with varying concentrations of MK13 (1.56–50 µM) or doxorubicin (DOX, Adriamycin, Pfizer) at doses ranging from 0.06 to 2 µg/mL using twofold serial dilutions. According to Pfizer (n.d.), doxorubicin reaches peak plasma concentrations of approximately 1 µM following intravenous administration [31]. Therefore, 1 µg/mL was selected as the clinically relevant concentration, while 2 µg/mL was used to represent a suprapharmacological dose [32]. After 48 h of treatment, cell viability was assessed using the MTT assay (3-(4,5-dimethylthiazol-2-yl)-2,5-diphenyltetrazolium bromide) (BioBasic, Canada). Briefly, a 5 mg/mL MTT stock solution was added to each well to achieve a final concentration of 10% (v/v), and plates were incubated to allow formazan crystal formation. Crystals were subsequently solubilized overnight using 10% SDS with 0.01 M HCl. To evaluate cell proliferation, an additional 96-well plate was seeded under the same conditions, and a parallel MTT assay was performed prior to treatment (time zero, T_0). These initial absorbance values were used for growth rate normalization as previously described [33]. Absorbance was measured at 570 nm using the LumiStar Omega spectrophotometer (BMG Labtech).

Morphological evaluations with fluorescent staining

To investigate the mode of cell death induced by MK13, cells were stained with the nuclear dyes Hoechst 33342 and propidium iodide (PI) (BioLegend, USA). Cells were treated with the IC_{90} concentration of MK13, and double staining was performed at 12, 24, and 48 h post-treatment, as previously described [34]. Briefly, the culture medium was removed from each well, and a staining solution containing 30 µM Hoechst 33342 and 1 µg/mL PI in PBS was added. Plates were incubated at room temperature for 15 min. Stained cells were visualized using a Zeiss Axio Observer fluorescence microscope, and images were captured with Zen Blue 3.11 Software.

Flow cytometry analyses

To elucidate the cellular mechanisms underlying MK13-induced cytotoxicity, flow cytometric analyses were conducted. CCLP1 cells were seeded in 6-well plates at a density of 3×10^5 cells per well and treated the following day with the IC_{90} concentration of MK13. After 12 and 24 h of exposure, cells were harvested and subjected to multiparametric flow cytometry using the Guava Muse Cell Analyzer. The following assay kits were employed according to the manufacturer's protocols: Annexin V & Dead Cell Kit (Cat. No. MCH100105) for apoptosis detection, Oxidative Stress Kit (Cat. No. MCH100111) for intracellular ROS measurement, and γH2AX Activation Kit (Cat. No. FCCS025153) for assessing DNA double-strand break formation.

Gene expression analysis with qPCR

CCLP1 cells were seeded on 6-well plates and the next day treated with IC_{90} dose and harvested for RNA isolation after 6 h of treatment with the MK13. Cellular RNA was isolated by using the NucleoSpin RNA Mini kit (MN Macherey-Nagel, Germany). Isolated RNA quality and quantity was measured by Nanodrop (Invitrogen, USA) and 1 microgram of each total RNA sample was used for cDNA synthesis with the iScript cDNA Synthesis Kit (BioRad, USA). For the gene expression analysis, qPCR method was used, 10 ng cDNA was used as template for each reaction that contains QuantiNova Syber Green Mix (Qiagen, Germany) and Applied Biosystem QuantStudio (Thermo Fisher Scientific, USA) device was used. Sample setup and analysis were accomplished using the macro file for each gene panel with the Light-Cycler 480 Software 1.5. Results were analyzed by using ΔΔCT method. GAPDH was used as a housekeeping gene and fold change of expression was

calculated according to it. Selected genes were classified into three groups as prosurvival genes (*AKT1, AKT2F, BAG4, BCL2, BCL2L2, BCL10, BCLXL, BIRC3, BIRC4, BIRC5, BIRC6, BMI1, CDC2, CDC20, CDK4, CDC25A, CDK2, MDM2, MCL1, NEK2, GRB2*), *pro-apoptotic genes (APAF1, BAD, BAX, BCLAF1, BAK1, BID, BIK, BIM, BMF, BNIP1, CASP2, CASP3, CASP4, CASP6, CASP8, CASP9, DR4, DR5, HRK, NOXA, FAS, PUMA RIPK2, XPA) and cellular stress-related genes (BAG3, BECN1, BNIP2, BNIP3, BNIP3L, CAT, ERCC1, ERCC3, GADD45A, GPX1, GSTP1, LIG4, MUTYH, NFKB, OGG1, PRDX1, RAD51, RAD52, SOD1, XRCC5*).

Statistical analysis

Two-way ANOVA was used for comparing the viability results with the control group. All statistical analyses were conducted using GraphPad Prism 9.4.1. Data for each independent replicate are presented as mean ± standard deviation.

Results

MK13 has a selectively effective on DOX-responsive cell line CCLP1

To evaluate the anticancer potential of the MK13 compound, a dose–response analysis was conducted using the MTT viability assay at concentrations ranging from 1.56 to 50 µM (Fig. 1a). The results demonstrated that both cell lines responded to MK13, albeit with distinct sensitivities. HUCCT1 cells exhibited a gradual decline in viability with increasing doses, whereas CCLP1 cells showed a sharp decrease even at lower concentrations. Interestingly, at higher doses (25–50 µM), both cell lines exhibited a similar reduction in viability, approximately 80%. In the case of CCLP1, slight increase in cell viability at higher doses may be attributed to three potential factors. First, MK13 might exhibit reduced solubility at elevated concentrations, which could limit its membrane

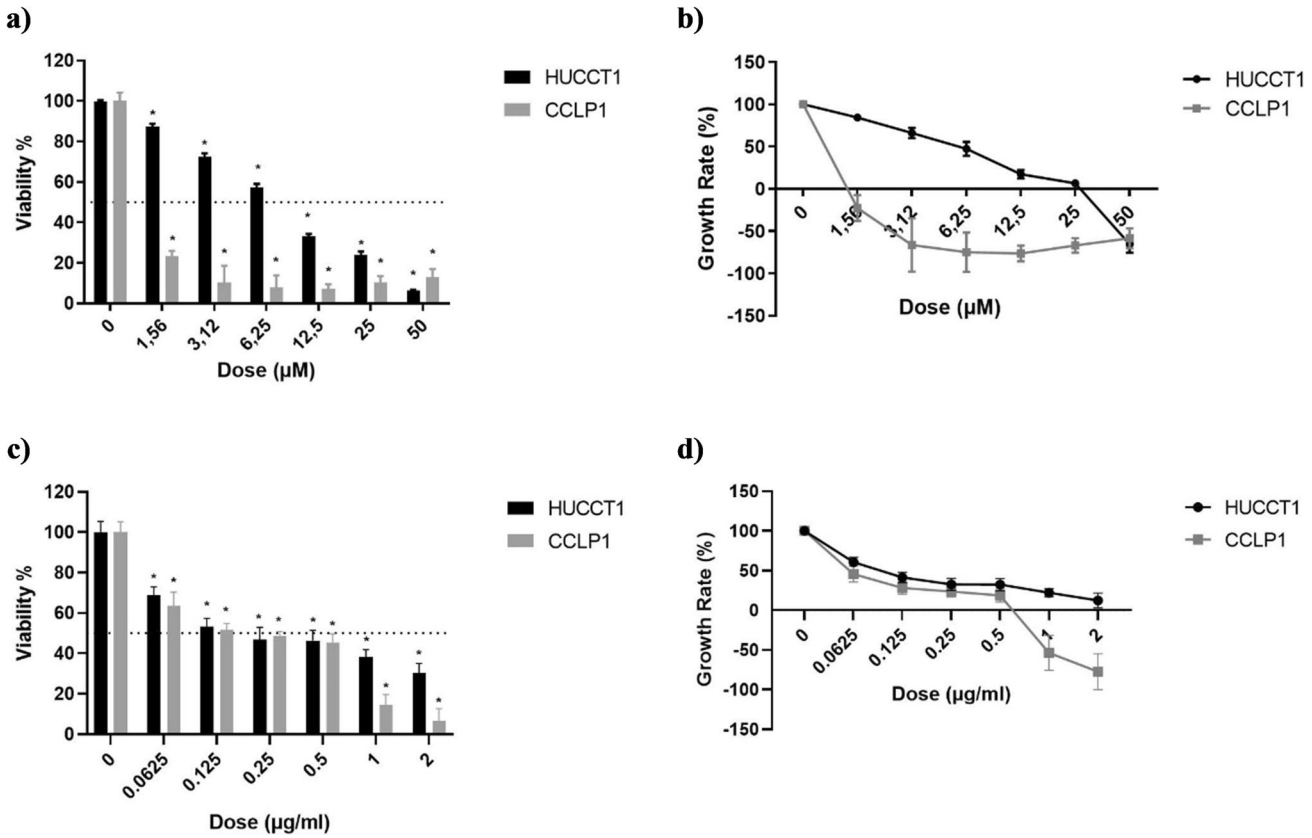

Fig. 1 MK13 has a cytotoxic effect on both cell lines as dose dependent manner. CCLP1 and HUCCT1 cells were treated with differential doses of either MK13 or DOX. MTT viability assay was conducted after 48 h treatment. Viability and growth gate was calculated as percentage as compared to untreated control cells. Data were visualized and analyzed with GraphPad Prisim 9.4.1. **a**, **b** Viability and growth rate graphs of MK13. **c**, **d** Viability and growth rate graphs of doxorubicin (DOX). Results are shown as the means and error bars indicate standard deviation of three biological replicates, each has triple technical replicates. Single asterisk (*) denotes the significance of comparison between untreated and treated groups at $p < 0.0001$ according to two-way ANOVA analysis

permeability. Second, MK13 itself may directly reduce MTT, (without needing dehydrogenase activity for reduction), thus leading to assay interference [35]. However, these effects were not observed for HUUCT cells. This discrepancy suggests a third explanation: that prolonged exposure to slightly elevated concentrations may trigger stress-adaptive responses in CCLP1, promoting increased proliferation despite treatment. Alternatively, intracellular aggregation of the compound at high doses might prevent its interaction with cellular targets which hinders compound from exerting its toxicity [36]. In addition to these, those results may be an artifact. However, even though they are artifacts, they do not make a confounding effect. Thus, although MK13 exhibited strong cytotoxic effects within the 3–12 µM range, higher concentrations may have activated specific adaptation mechanisms. These types of response patterns are referred to as nonmonotonic dose–response curves, often characterized by distinct response phases such as the biphasic pattern observed in CCLP1 [37]. This biphasic behavior was also evident in the growth rate profile (Fig. 1b). Overall, CCLP1 cells were significantly more sensitive to MK13, exhibiting markedly lower IC_{50} and GI_{50} values (1.02 ± 0.03 µM and 0.64 ± 0.07 µM, respectively), nearly ten-fold lower than those observed in HUCCT1 (7.97 ± 0.95 µM and 5.88 ± 1.14 µM) (Table 1).

Doxorubicin (DOX), a well-established chemotherapeutic quinone widely used in clinical practice, served as the positive control. The results demonstrated that HUCCT1 cells were relatively less sensitive to DOX as compared to CCLP1 cells (Fig. 1c, d). Notably, even at a supraphamacological concentration (2 µg/mL), more than a quarter of the HUCCT1 cells remained viable. The growth curve of HUCCT1 cells did not decline below the cytotoxic threshold, whereas CCLP1 cells exhibited a similar trend but showed a significant decrease in viability at concentrations above 0.5 µg/mL. IC_{50} and GI_{50} doses for DOX was calculated similar for HUCCT (4.94 ± 1.46 µg/mL and 0.10 ± 0.02 µg/mL) and CCLP1 (4.67 ± 1.11 µg/mL and 0.06 ± 0.01 µg/mL) while IC_{90}, TGI and LD_{50} doses of HUCCT were above 2 µg/mL (Table 2).

Table 1 Calculated doses for iCCA cell lines treated with MK13 for 48 h

MK13 (µM)	HUCCT1	CCLP1
IC_{50}	7.97 ± 0.95	1.02 ± 0.03
IC_{90}	44.90 ± 0.27	5.98 ± 4.61
GI_{50}	5.88 ± 1.14	0.64 ± 0.07
TGI	27.18 ± 0.95	1.29 ± 0.14
LD_{50}	45.03 ± 2.29	3.83 ± 2.21

Table 2 Calculated doses for iCCA cell lines treated with DOX for 48 h

DOX (µg/mL)	HUCCT1	CCLP1
IC_{50}	4.94 ± 1.46	4.67 ± 1.11
IC_{90}	> 2	42.30 ± 6.40
GI_{50}	0.10 ± 0.02	0.06 ± 0.01
TGI	> 2	0.64 ± 0.06
LD_{50}	> 2	1.25 ± 0.33

Overall, these data indicate that DOX-responsive CCLP1 cells are significantly more sensitive to MK13 treatment. Therefore, subsequent mechanistic and biochemical analyses were conducted on only this cell line.

MK13 triggers apoptotic cell death on both cell line

A morphological evaluation was conducted to investigate MK13-induced cell death using a fluorescence-based staining approach. To assess the mode of cell death, CCLP1 and HUCCT1 cells were treated with corresponding IC_{90} concentrations of MK13 for 48h. Fluorescent staining was performed at multiple time points (12, 24, and 48h) to examine the time-dependent response. Two nuclear fluorescent dyes, Hoechst 33342 and propidium iodide (PI), were used to differentiate apoptotic and necrotic nuclear morphologies. Hoechst 33342 is a membrane-permeable dye that stains all nuclei, while PI is impermeable to intact membranes and thus only stains nuclei of cells with compromised membrane integrity. Consequently, PI-positive nuclei indicate necrotic or late-stage apoptotic cells (secondary necrotic cells). During apoptosis, the chromatin condenses, and the nucleus either shrinks as a whole or fragmented. A cell exhibiting both PI positivity and pyknotic or fragmented morphology suggests the progression into secondary necrosis/late-stage apoptosis observed in vitro when efferocytosis is absent [38, 39].

MK13 treatment of CCLP1 cells led to a time-dependent increase in pyknotic nuclei, indicating apoptotic cell death. Nuclear fragmentation, or karyorrhexis, was also observed. In addition, a marked reduction in cell confluence was noted over time following MK13 treatment as compared to control cells (Figs. 2, 3). Fluorescence microscopy confirmed that MK13 induces apoptotic cell death, as evidenced by the increasing number of pyknotic nuclei over time and the corresponding decrease in total cell number. After 24 h of treatment, secondary necrosis was observed, indicated by PI-positive pyknotic nuclei. In contrast, the mode of cell death in HUCCT1 cells appeared to differ from that happens in CCLP1 cells. Although pyknotic nuclei were present, secondary necrosis—marked by membrane disruption and PI uptake—was largely absent. Most cells remained in early

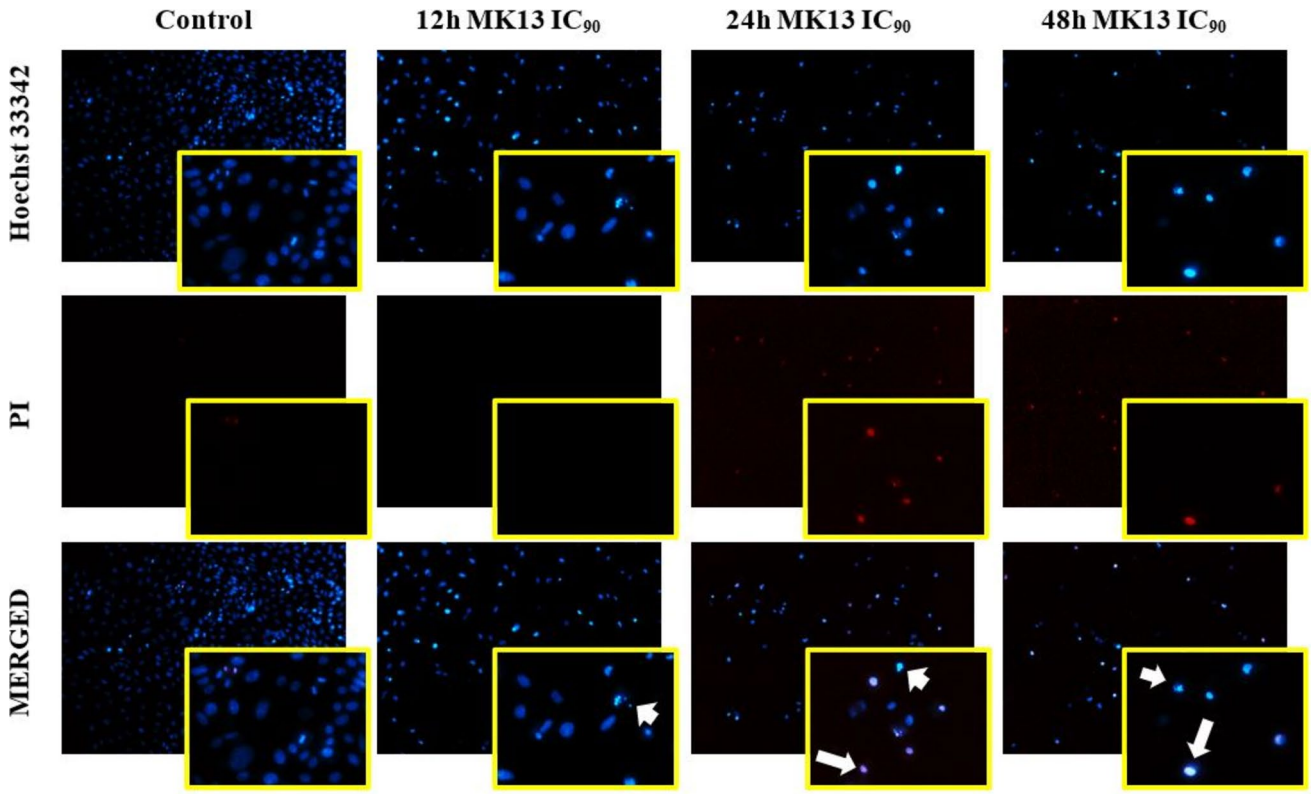

Fig. 2 Apoptotic nuclear morphology was observed after MK13 treatment of CCLP1 cells. CCLP1 cells were treated with IC_{90} dose of MK13 and stained with Hoechst 33342 and PI double fluorescent dyes after 12–24–48 h. Images taken with Zeiss Axio Observer 10×objective, and the yellow framed images taken with 40×objective then analyzed with Zen Blue 3.11 Software. Short arrows point early apoptotic nuclei evident with PI negativity and pyknosis; long arrows point late apoptotic nuclei evident with PI positivity with pyknosis. Blue: Hoechst 33342 dye, red: PI

stages of apoptosis, with only a small proportion progressing to secondary necrosis (Fig. 3). In summary, MK13 was shown to induce apoptotic cell death in both cell lines at IC_{90} concentrations in a time-dependent manner, with notable differences in the extent of secondary necrosis between CCLP1 and HUCCT1 cells.

Apoptosis triggered by MK13 is caused by DNA Damage which is independent of oxidative stress

Flow cytometry analysis was performed to elucidate the cellular responses to MK13 treatment. Cells were treated with IC_{90} concentration, and apoptotic progression was assessed at 12 and 24 h, the time points previously shown to exhibit apoptotic features via fluorescence microscopy (Fig. 2). To ensure consistency, the same population of cells was divided appropriately for each flow cytometry assay. Phosphatidylserine translocation analysis via annexin V-FITC staining revealed that approximately one-fourth of the cell population had progressed to late apoptosis, while the total proportion of apoptotic cells exceeded 50% after 12 h of treatment (Fig. 4a), consistent with the observations from nuclear staining (Fig. 2). Although no significant increase in total apoptotic cell count was observed between 12 and 24h, nearly all dead cells at both time points were Annexin V-FITC-positive, indicating the phosphatidylserine translocation. This suggests that MK13 does not induce uncontrolled or primary necrotic cell death but rather initiates a regulated apoptotic pathway. Therefore, the apoptotic nuclear morphology identified by fluorescence microscopy was corroborated by biochemical analysis, supporting the conclusion that MK13 induces apoptotic cell death.

NQ derivatives are commonly associated with rapid reactive oxygen species (ROS) generation and thereby DNA damage [40–42]. To explore whether these mechanisms contribute to MK13-induced cytotoxicity, oxidative stress and DNA damage levels were assessed via flow cytometry. ROS analysis demonstrated no significant increase following MK13 treatment either at 12 or 24 h (8.47% and 5.84%, respectively; Fig. 4b). In contrast, DNA damage, as indicated by the phosphorylation of histone H2AX (γH2AX), progressively increased from 22.6% at 12 h to 36.9% at 24 h (Fig. 4c). These results suggest that MK13-induced DNA damage is not driven by oxidative stress but may instead

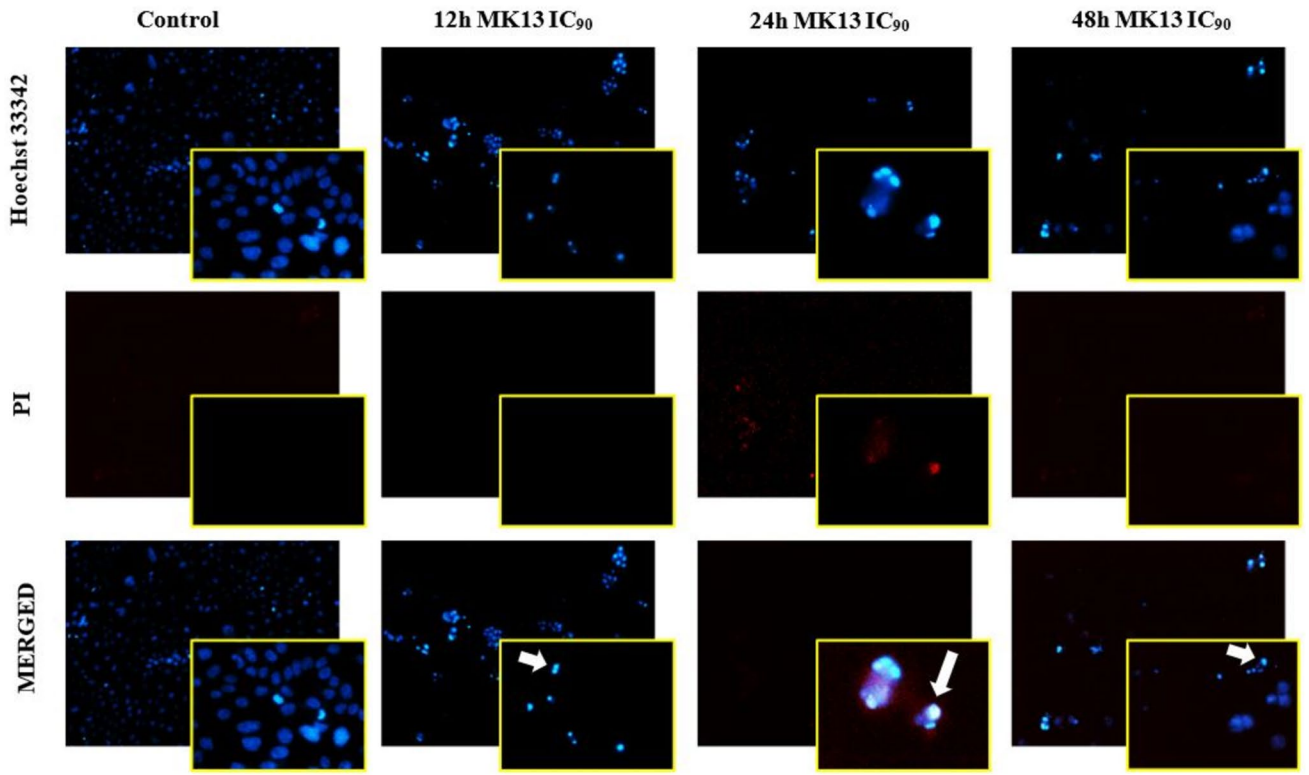

Fig. 3 Apoptotic nuclear morphology was observed after MK13 treatment of HUCCT1 cells. HUCCT1 cells were treated with IC_{90} dose of MK13 and stained with Hoechst 33342 and PI double fluorescent dyes after 12–24–48 h. Images taken with Zeiss Axio Observer 10×objective, and the yellow framed images taken with 40×objective then analyzed with Zen Blue 3.11 Software. Short arrows point early apoptotic nuclei evident with PI negativity and pyknosis; long arrows point late apoptotic nuclei evident with PI positivity. Blue: Hoechst 33342 dye, red: PI

result from a direct interaction between MK13 and DNA, potentially through the formation of DNA crosslinks.

Pro-apototic and prosurvival genes are differentially regulated after MK13 exposure

To assess gene expression changes following MK13 treatment, quantitative PCR (qPCR) analysis was performed. Target genes were categorized into three groups: prosurvival, pro-apoptotic, and cellular stress-related genes. Cells were treated with the IC_{90} concentration of MK13 for 6h, after which gene expression levels were analyzed (Fig. 5a). The results showed that most prosurvival genes were downregulated following MK13 treatment. In contrast, several pro-apoptotic genes responded, even after this relatively short exposure. Among the upregulated genes were *APAF1, PUMA, NOXA, BAX*, and notably *DR5* that are all well-known apoptosis-inducers, while *CASP2, CASP6, CASP8, BCLAF1, BID*, and *BIK* were downregulated (Fig. 5b). Genes associated with oxidative stress did not show significant changes upon MK13 exposure. Similarly, most DNA damage repair genes—*ERCC3, XRCC5, RAD51*, and *RAD52*—remained unaffected, except for *ERCC1,* which showed a measurable response (Fig. 5c). In summary, MK13 treatment led to early transcriptional changes favoring apoptosis. *BAX* and *DR5* were identified as the most prominently upregulated genes, suggesting their potential involvement in MK13-induced apoptotic signaling. In contrast, *CASP8* mRNA was significantly downregulated following treatment. Given that caspase-8 and DR5 are both indispensable components of the extrinsic apoptosis pathway—with DR5 serving as a death receptor and caspase-8 functioning as a key initiator caspase—we further examined caspase-8 protein expression to assess activation status. Since caspases are activated through proteolytic cleavage rather than solely transcriptional regulation, western blot analysis was performed. Notably, caspase-8 protein was undetectable in both MK13-treated and control groups, suggesting a lack of involvement of the extrinsic pathway in this context (Supplementary Material). These findings support the hypothesis that MK13 induces apoptosis through a caspase-8–independent mechanism, likely involving the intrinsic (mitochondrial) apoptotic pathway.

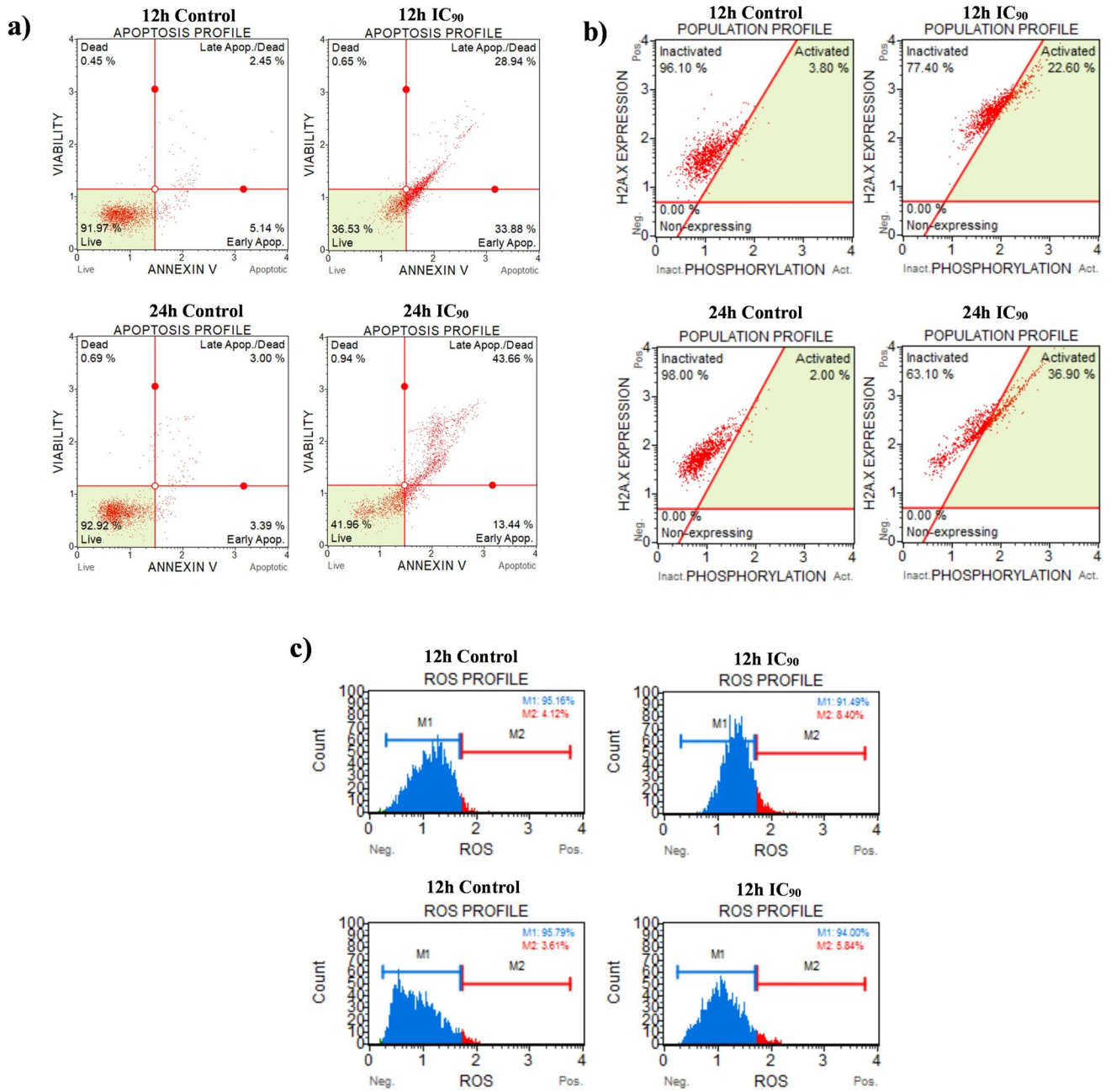

Fig. 4 Apoptotic cell death triggered by MK13 treatment was associated with DNA damage. CCLP1 cells were treated with IC_{90} dose of MK13 for 12–24 h of incubation. After treatment, cells were harvested and analyzed with Guava MUSE Cell Analyzer flow cytometry for **a** phosphatidylserine translocation, **b** oxidative stress, **c** H2AX activation

Discussion

CCA remains a highly aggressive malignancy with limited therapeutic options and poor clinical outcomes, urging the need for novel treatment strategies. NQ derivatives have attracted considerable interest due to their diverse anticancer mechanisms, including the induction of apoptosis and oxidative stress. In this study, we investigated the anticancer potential of MK13, a naphthoquinone-based compound, in intrahepatic-CCA (iCCA) using two cell lines: CCLP1 and HUCCT1. Both cell lines responded to MK13 treatment, although CCLP1 cells were significantly more sensitive in terms of viability reduction and growth inhibition (Fig. 1). This selective cytotoxicity was particularly evident at lower concentrations (1.56–12.5 µM) and was reflected in the IC_{50} and GI_{50} values. Notably, when compared with doxorubicin—a clinically used chemotherapeutic agent—MK13 exhibited superior efficacy in CCLP1 cells. Although

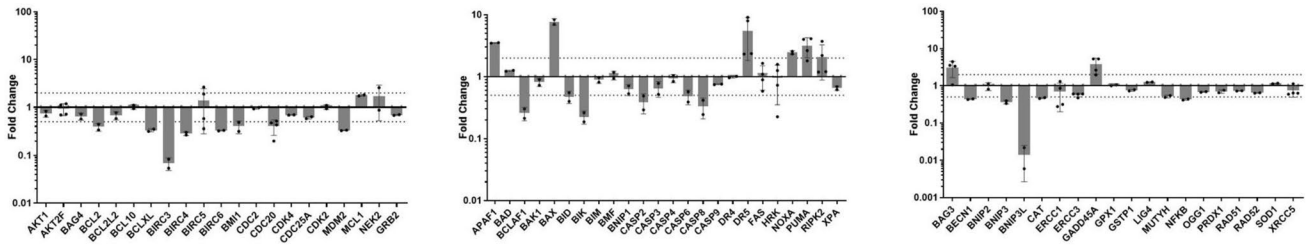

Fig. 5 Differential gene expression analysis with qPCR. CCLP1 cells were treated with MK13 IC_{90} dose for 6 h then total RNA was extracted and used for cDNA synthesis. The analyzed genes were divided into three major groups according to their biological function: **a** prosurvival genes, **b** pro-apoptotic genes, **c** cellular stress-related genes. Data were visualized with GraphPad Prisim 9.4.1. Bar graphs depict the mean of the fold change while error bars indicate the standard deviation. Single data points were represented on the bars while each biological replicate has two technical replicates. The fold change was calculated using ΔΔCT method and *GAPDH* was used as housekeeping gene. Genes that have ≥ 2-fold change were excepted as upregulated whereas the ones that have ≤ 1/2-fold change were excepted as downregulated

doxorubicin reduced viability in both cell lines, HUCCT1 cells remained relatively resistant, with over 25% viability even at a suprapharmacological dose of 2 µg/mL. In contrast, MK13 induced potent cytotoxicity specifically in CCLP1 cells, which also exhibited sensitivity to doxorubicin, implying its strong efficacy in the treatment-responsive iCCA model. The recent studies increasingly highlight the therapeutic relevance of quinones in CCA treatment. Several quinone derivatives, including plumbagin, rhinacanthin-C, hypocrellin A, thymoquinone, and shikonin, have demonstrated notable anticancer effects by suppressing proliferation and inducing apoptosis in CCA models [22–27]. In this context, MK13 showed promising efficacy particularly in a doxorubicin-sensitive CCA cell line, further reinforcing the therapeutic potential of quinones in CCA treatment.

Based on this differential sensitivity, subsequent mechanistic experiments were performed primarily in CCLP1 cells. Nuclear staining with Hoechst 33342 and propidium iodide (PI) revealed hallmark features of apoptosis, including chromatin condensation and pyknosis, following MK13 treatment at the IC_{90} dose (Fig. 2). Moreover, the number of apoptotic and PI-positive nuclei increased over time, suggesting progression toward secondary necrosis, a phenomenon consistent with apoptotic cell death in vitro [38, 39]. These morphological findings were further corroborated by flow cytometry analysis demonstrating phosphatidylserine externalization (Fig. 4a), confirming MK13-induced apoptosis.

The distinct origins and clinical backgrounds of CCLP1 and HUCCT1 cells are likely to contribute to their differential drug responses. CCLP1 cells were derived from a primary intrahepatic-cholangiocarcinoma in a patient who had previously received 5-fluorouracil and leucovorin treatment, while HUCCT1 cells originated from a moderately differentiated intrahepatic bile duct adenocarcinoma suggesting a more aggressive and treatment-naïve tumor phenotype [43, 44]. At the molecular level, one of the key distinguishing features is their TP53 mutation profiles. CCLP1 harbors a nonsense R306X mutation, introducing a premature termination codon that triggers nonsense-mediated mRNA decay, resulting in functional loss of p53 tumor suppressor activity [40, 41]. In contrast, HUCCT1 carries the R175H missense mutation, a well-characterized gain-of-function (GOF) alteration [42]. This mutation not only disrupts wild-type p53 function but also confers oncogenic properties, including impaired G2/M checkpoint regulation, resistance to apoptosis, and increased genomic instability [45–47]. In addition, $p53^{R175H}$ acts in a dominant-negative manner, suppressing transcription of canonical p53 target genes such as *BAX, PUMA, NOXA, BCL2*, and *CDKN1A* (p21) [48].

Beyond TP53, other molecular differences may also influence drug sensitivity. These include variations in apoptotic signaling pathways, antioxidant capacity, and drug efflux transporter activity. For example, HUCCT1 cells harbor an activating *KRAS* mutation, which further amplifies oncogenic signaling via the MAPK and PI3K pathways. This constitutive KRAS activity has been associated with resistance to certain targeted therapies, particularly those acting upstream (e.g., EGFR inhibitors), and may contribute to the elevated survival capacity and reduced drug sensitivity [49, 50]. Together, these intrinsic differences may explain the observed selectivity of MK13, and further transcriptomic or proteomic profiling of these cell lines could provide deeper insights into the mechanisms underlying their distinct responses.

NQs are widely known to exert anticancer effects primarily through the induction of oxidative stress by elevating intracellular ROS levels, as demonstrated by compounds like plumbagin and other synthetic derivatives [51–56]. However, in this study, MK13 did not induce significant ROS accumulation in CCLP1 cells, even at IC_{90} concentration (Fig. 4b), suggesting a ROS-independent mechanism of cytotoxicity. In contrast, an unpublished study by our group showed a nearly tenfold ROS increase in CCLP1 cells

treated with another synthetic NQ derivative, highlighting the compound-specific variation among NQs. The modest ROS elevation observed with MK13 was thus considered biologically nonsignificant in the context of apoptosis. On the other hand, MK13-treated CCLP1 cells exhibited clear signs of DNA damage, evidenced by increased γ-H2AX phosphorylation over time as detected by flow cytometry (Fig. 4c). This finding aligns with previous studies showing that many NQs can directly induce DNA damage [57]. Given the lack of ROS elevation, it is plausible that MK13 causes DNA damage through direct nuclear interaction, similar to the action mechanism of the quinone-based chemotherapeutic agent DOX [58]. Further supporting this, we observed upregulation of *GADD45A*, a key genotoxic stress responder that plays a critical role in DNA damage repair and cell cycle arrest. GADD45A is known to interact with central regulatory proteins such as p53 and PCNA, thereby influencing the cellular response to DNA damage and stress [59]. Its expression has been linked to both enhanced and reduced chemosensitivity, depending on the context; for instance, GADD45A downregulation was associated with increased cisplatin sensitivity in melanoma [60]. In our case, although *GADD45A* upregulation supports the presence of DNA damage, the lack of change in the expression of other DNA repair-related genes suggests a partial or inadequate DNA repair response. Lastly, the p53 mutation status of CCLP1 cells provides important context for their heightened drug sensitivity. These cells harbor a truncating R306X mutation, leading to a complete loss of functional p53 protein [40, 41]. As p53 is essential for coordinating the DNA damage response, its truncation in CCLP1 cells (R306X) likely contributes to the accumulation of unrepaired DNA lesions. This loss-of-function mutation renders CCLP1 cells highly sensitive to MK13, with pronounced DNA damage observed even at low doses [45, 46].

Among the apoptosis-related genes analyzed, *DR5* (Death Receptor 5) emerged as one of the most strongly upregulated genes following MK13 treatment, alongside the pro-apoptotic gene *BAX* (Fig. 5b). DR5 is a crucial component of the extrinsic apoptosis pathway, mediating apoptotic signals via death ligand binding and subsequent formation of the death-inducing signaling complex (DISC). This upregulation suggests that, in addition to activating the intrinsic pathway, evidenced by BAX upregulation and BCL2 downregulation, MK13 may also sensitize cells to extrinsic apoptotic stimuli [48, 51, 52]. A similar observation was reported in a study using DOX in lung and colorectal cancer cell lines, where DR5 expression was upregulated following treatment, and its combination with a DR5 agonist significantly enhanced cytotoxic activity [61, 62]. Additional studies have shown that DR5 upregulation can potentiate the apoptotic response of cancer cells to various therapeutic agents. For example, gefitinib, an EGFR inhibitor, has been demonstrated to increase DR5 expression, thereby enhancing the sensitivity of non-small cell lung cancer (NSCLC) cells to extrinsic apoptosis. This effect is closely associated with BAX activation, leading to augmented apoptotic signaling [63]. Similarly, the combination of the triterpenoid pristimerin with taxol has been shown to induce cell death in cervical cancer cells through a mechanism involving both DR5 upregulation and BAX activation, underscoring the interconnected roles of these pathways in mediating drug response [64]. Moreover, the expression of DR5 has been correlated with the efficacy of chemotherapy in NSCLC patients, where high levels of DR5 and its interaction with c-FLIP proteins were associated with improved drug-induced apoptosis [65, 66]. This suggests that DR5 not only serves as a marker for drug response but also plays an active role in mediating the apoptotic effects of chemotherapeutic agents through pathways involving BAX. Thus, MK13 may not only promote activation of the intrinsic apoptotic pathway leading to cell death, but also potentially sensitize CCLP1 cells to external stimuli, increasing the likelihood of engaging the extrinsic apoptotic pathway under appropriate conditions.

However, when analyzing the expression profile in more detail, we observed a notable downregulation of caspase-8 (*CASP8)* at the gene expression level following MK13 treatment. Caspase-8 is a key initiator caspase required for extrinsic apoptosis via DR5 signaling; it is responsible for initiating the caspase cascade upon recruitment to the DISC [67]. Since caspases are tightly regulated at the post-translational level, changes in mRNA expression may not accurately reflect their functional activity. Therefore, despite observing a downregulation of *CASP8* transcripts, we aimed to assess whether caspase-8 was present or activated at the protein level. To this end, we performed a western blot analysis after 6 and 12 h of treatment with MK13 at IC_{90} concentration, focusing on both full-length and cleaved caspase-8. Surprisingly, no caspase-8 protein was detectable at either point, not even in the untreated control group, suggesting that caspase-8 is either not expressed or post-translationally silenced in CCLP1 cells (Supplementary Material). Moreover, *BID*, a BH3-only Bcl-2 family protein that serves as a crucial link between extrinsic and intrinsic apoptosis, was also found to be transcriptionally downregulated (Fig. 5b). Under normal conditions, caspase-8 cleaves BID into truncated BID (tBID), which translocate to mitochondria to amplify apoptosis via mitochondrial outer membrane permeabilization and BAX/BAK activation. The downregulation of both *CASP8* and *BID* suggests that not only is the extrinsic apoptotic pathway inactive, but also that crosstalk to the intrinsic pathway is compromised. *DR5* upregulation may serve more as a stress marker rather than a functional pro-apoptotic trigger [67, 68]. In contrast, the observed upregulation of *PUMA, NOXA*, and *BAX*, alongside the downregulation of the antiapoptotic gene *BCL2*,

indicates activation of the intrinsic apoptotic pathway via a caspase-8-independent mechanism. As p53-regulated BH3-only proteins, PUMA and NOXA antagonize antiapoptotic Bcl-2 family members, promoting BAX activation and mitochondrial outer membrane permeabilization [69, 70]. These findings suggest that intrinsic apoptosis may still be engaged through direct mitochondrial signaling, even in the absence of functional extrinsic input. These results support the conclusion that MK13-induced apoptosis in CCLP1 cells proceeds independently of DR5–CASP8–BID signaling, and is likely driven predominantly through the intrinsic, mitochondrial pathway via BAX activation and BCL2 suppression.

In conclusion, this study highlights the anticancer potential of MK13 as a potent inducer of intrinsic apoptosis, primarily through the induction of severe DNA damage. The apoptotic response appears to be driven by mitochondrial signaling, independent of ROS accumulation or canonical extrinsic pathway activation. Future studies should be conducted to evaluate the compounds *in vivo* antitumoral activity and therapeutic responsiveness.

Supplementary Information The online version contains supplementary material available at https://doi.org/10.1007/s12032-025-02927-7.

Acknowledgements This publication is based upon work from the European Network for the Study of Cholangiocarcinoma and the COST Action Precision-BTC-Network CA22125, supported by COST (European Cooperation in Science and Technology; www.cost.eu). The authors of Koc University gratefully acknowledge the use of the services and facilities of the Koç University Research Center for Translational Medicine (KUTTAM).

Author contributions Conceptualization, Zeliha GOKMEN and Engin ULUKAYA; Data curation, Gizem BULUT, Merve KAYIS and Dilan GEZEN; Investigation, Chiara RAGGI and Engin ULUKAYA; Methodology, Zelal ADIGUZEL, Chiara RAGGI and Engin ULUKAYA; Resources, Zelal ADIGUZEL and Engin ULUKAYA; Supervision, Engin ULUKAYA; Visualization, Gizem BULUT; Writing—original draft, Gizem BULUT; Writing—review & editing, Gizem BULUT, Zelal ADIGUZEL, Chiara RAGGI and Engin ULUKAYA.

Funding This study was funded by the Scientific Research Projects Coordination Unit of Istanbul University-Cerrahpasa (Project numbers: FBA-2024-37858).

Data availability The data that support the findings of this study are available from the corresponding author upon reasonable request.

Declarations

Conflict of interest The authors declare no conflict of interest.

References

1. Ilyas SI, Affo S, Goyal L, Lamarca A, Sapisochin G, Yang JD, Gores GJ. Cholangiocarcinoma—novel biological insights and therapeutic strategies. Nat Rev Clin Oncol. 2023;20(7):470–86.
2. Xiao Y, Shan ZJ, Yang JF, Len JJ, Yu YH, Yang ML. Nephrometric scoring system: recent advances and outlooks. Urol Oncol Semin Original Investig. 2023;41(1):15–26.
3. Benavides M, Antón A, Gallego J, Gómez MA, Jiménez-Gordo A, La Casta A, et al. Biliary tract cancers: SEOM clinical guidelines. Clin Transl Oncol. 2015;17(12):982–7. https://doi.org/10.1007/s12094-015-1436-2.
4. Yang JQ, Wang XG, Wu B. Incidence trend and prognosis of intrahepatic cholangiocarcinoma: a study based on the SEER database. Transl Cancer Res. 2023;12(11):3007–15. https://doi.org/10.21037/tcr-23-1278.
5. Bañales JM, Marin JJG, Lamarca A, Rodrigues PM, Khan SA, Roberts LR, et al. Cholangiocarcinoma 2020: the next horizon in mechanisms and management. Nat Rev Gastroenterol Hepatol. 2020;17(9):557–88. https://doi.org/10.1038/s41575-020-0310-z.
6. Qurashi M, Vithayathil M, Khan SA. Epidemiology of cholangiocarcinoma. Eur J Surg Oncol. 2023. https://doi.org/10.1016/j.ejso.2023.107064.
7. Khan SA, Thomas HC, Davidson BR. Cholangiocarcinoma: current treatment algorithms. Hepatology. 2021;73(2):797–810. https://doi.org/10.1016/s0140-6736(05)67530-7.
8. Pellino A, Loupakis F, Cadamuro M, Dadduzio V, Fassan M, Guido M, et al. Precision medicine in cholangiocarcinoma. Transl Gastroenterol Hepatol. 2018;3:40. https://doi.org/10.21037/tgh.2018.07.02.
9. Izquierdo-Sanchez L, Lamarca A, La Casta A, Buettner S, Utpatel K, Klümpen HJ, et al. Cholangiocarcinoma landscape in Europe: diagnostic, prognostic and therapeutic insights from the ENSCCA Registry. J Hepatol. 2022;76(5):1109–21. https://doi.org/10.1016/j.jhep.2021.12.010.
10. Mavros MN, Economopoulos KP, Alexiou VG, Pawlik TM. Treatment and prognosis for patients with intrahepatic cholangiocarcinoma: systematic review and meta-analysis. JAMA Surg. 2014;149(6):565–74. https://doi.org/10.1001/jamasurg.2013.5137.
11. Wada Y, Shimada M, Yamamura K, Toshima T, Banwait JK, Morine Y, Goel A. A transcriptomic signature for risk-stratification and recurrence prediction in intrahepatic cholangiocarcinoma. Hepatology. 2021;74(3):1371–83.
12. Chen B, Mao Y, Li J, Zhao Z, Chen Q, Yu Y, Xie X. Predicting very early recurrence in intrahepatic cholangiocarcinoma after curative hepatectomy using machine learning radiomics based on CECT: a multi-institutional study. Comput Biol Med. 2023;167:107612.
13. Moris D, Palta M, Kim C, Allen PJ, Morse MA, Lidsky ME. Advances in the treatment of intrahepatic cholangiocarcinoma: an overview of the current and future therapeutic landscape for clinicians. CA Cancer J Clin. 2023;73(2):198–222.
14. Khosla D, Misra S, Chu PL, Guan P, Nada R, Gupta R, et al. Cholangiocarcinoma: recent advances in molecular pathobiology and therapeutic approaches. Cancers. 2024;16(4):801. https://doi.org/10.3390/cancers16040801.
15. Gaspar A, Matos MJ. Naphthoquinones: an overview of their medicinal chemistry. Eur J Med Chem. 2015;97:624–61. https://doi.org/10.1016/j.ejmech.2014.08.061.
16. Navarro-Tovar G, Vega-Rodríguez S, Leyva E, Loredo-Carrillo S, de Loera D, López-López LI. The relevance and insights on 1,4-naphthoquinones as antimicrobial and antitumoral molecules: a systematic review. Pharmaceutics. 2023;16(4):496. https://doi.org/10.3390/ph16040496.
17. Wang JR, Shen GN, Luo YH, Piao XJ, Zhang Y, Wang H, et al. 2-(4-Methoxyphenylthio)-5,8-dimethoxy-1,4-naphthoquinone induces apoptosis via ROS-mediated MAPK and STAT3 signaling pathway in human gastric cancer cells. J Chemother. 2019;31(4):214–26. https://doi.org/10.1080/1120009x.2019.1610832.

18. Liu C, Shen GN, Luo YH, Piao XJ, Jiang XY, Meng LQ, et al. Novel 1,4-naphthoquinone derivatives induce apoptosis via ROS-mediated p38/MAPK, Akt and STAT3 signaling in human hepatoma Hep3B cells. Int J Biochem Cell Biol. 2018;96:9–19. https://doi.org/10.1016/j.biocel.2018.01.004.
19. Jali BR, Behura R, Barik SR, Parveen S, Mohanty SP, Das RA. A brief review: biological implications of naphthoquinone derivatives. Res J Pharm Technol. 2018;11(8):3698–702. https://doi.org/10.5958/0974-360X.2018.00679.0.
20. Karakaş ZD, Akar RO, Gokmen Z, Deniz NG, Ulukaya E. A novel 1,4-naphthoquinone-derived compound induces apoptotic cell death in breast cancer cells. Turk J Biol. 2019;43(4):256–63. https://doi.org/10.3906/biy-1901-19.
21. Adacan K, Gokmen Z, Akar RO, Ozyıldız Z, Dinçer H, Karakaş D, Ulukaya E. Synthesis, characterization and apoptosis capabilities of a novel naphthoquinone-derived compound in triple-negative breast cancer. ChemistrySelect. 2023;43(8):e202301955. https://doi.org/10.1002/slct.202301955.
22. Buranrat B, Utsintong M. Plumbagin suppresses growth, induces apoptosis, and inhibits migration in cholangiocarcinoma via reactive oxygen species generation and mitochondrial function. Pharmacogn Mag. 2023;19(2):325–35. https://doi.org/10.1177/09731296231158221.
23. Boueroy P, Saensa-Ard S, Siripong P, Kanthawong S, Hahnvajanawong C. Rhinacanthin-C extracted from *Rhinacanthus nasutus* (L.) inhibits cholangiocarcinoma cell migration and invasion by decreasing MMP-2, uPA, FAK and MAPK pathways. Asian Pac J Cancer Prevention (APJCP). 2018;19(12):3605–13. https://doi.org/10.3155/APJCP.2018.19.12.3605.
24. Chen B, Chen Q, Lu M, Zou E, Lin G, Yao J, Wu L. Hypocrellin A against intrahepatic cholangiocarcinoma via multi-target inhibition of the PI3K-AKT-mTOR, MAPK, and STAT3 signaling pathways. Phytomedicine. 2024;135:156022.
25. Xu D, Ma Y, Zhao B, Li S, Zhang YU, Pan S, Jiang H. Thymoquinone induces G2/M arrest, inactivates PI3K/Akt and nuclear factor-κB pathways in human cholangiocarcinomas both in vitro and in vivo. Oncol Rep. 2014;31(5):2063–70.
26. Abdualmjid RJ, Sergi CM. Mitochondrial dysfunction and induction of apoptosis in hepatocellular carcinoma and cholangiocarcinoma cell lines by thymoquinone. Int J Mol Sci. 2022;23(23):14669. https://doi.org/10.3390/ijms232314669.
27. Liu C, Xuan LQ, Li K, Feng Z, Lv C, Li XJ, Ji XD, Wan R, Shen J. Shikonin inhibits cholangiocarcinoma cell line QBC939 by regulating apoptosis, proliferation, and invasion. Cell Transplant. 2021;30:963689720979162. https://doi.org/10.1177/0963689720979162.
28. Gokmen Z, Onan ME, Deniz NG, Karakas D, Ulukaya ES. Synthesis and investigation of cytotoxicity of new N-and S, S-substituted-1,4-naphthoquinone (1,4-NQ) derivatives on selected cancer lines. Synth Commun. 2019;49(21):3008–16. https://doi.org/10.1080/00397911.2019.1655057.
29. Gokmen Z, Alahmad H. Novel amino- and thio(substituted)-1,4-naphthoquinone (NQ) compounds: synthesis and characterization. Phosphorus Sulfur Silicon Relat Elem. 2020;195(9):718–25. https://doi.org/10.1080/10426507.2020.1755973.
30. Deniz NG, Ibis C, Gokmen Z, Stasevych M, Novikov V, Komarovska-Porokhnyavets O, Ozyurek M, Guclu K, Karakas D, Ulukaya E. Design, synthesis, biological evaluation, and antioxidant and cytotoxic activity of heteroatom-substituted 1,4-naphtho- and benzoquinones. Chem Pharm Bull. 2015;63(12):1029–39. https://doi.org/10.1248/cpb.c15-00607.
31. Pfizer. (n.d.). Doxorubicin hydrochloride: clinical pharmacology. Pfizer Medical Information. https://www.pfizermedicalinformation.com/doxorubicin/clinical-pharmacology.
32. Siebel C, Lanvers-Kaminsky C, Würthwein G, Hempel G, Boos J. Bioanalysis of doxorubicin aglycone metabolites in human plasma samples–implications for doxorubicin drug monitoring. Sci Rep. 2020;10(1):18562.
33. Monks A, Scudiero D, Skehan P, Shoemaker R, Paull K, Vistica D, et al. Feasibility of a high-flux anticancer drug screen using a diverse panel of cultured human tumor cell lines. J Natl Cancer Inst (JNCI). 1991;83(11):757–66. https://doi.org/10.1093/jnci/83.11.757.
34. Erkisa M, Ari F, Ulku I, Khodadust R, Yar Y, Yagci Acar H, Ulukaya E. Etoposide loaded SPION-PNIPAM nanoparticles improve the in vitro therapeutic outcome on metastatic prostate cancer cells via enhanced apoptosis. Chem Biodivers. 2020;17(11):e2000607. https://doi.org/10.1002/cbdv.202000607.
35. Ulukaya E, Colakogullari M, Wood EJ. Interference by anti-cancer chemotherapeutic agents in the MTT-tumor chemosensitivity assay. Chemotherapy. 2004;50(1):43–50. https://doi.org/10.1159/000077285.
36. Chern YJ, Tai IT. Adaptive response of resistant cancer cells to chemotherapy. Cancer Biol Med. 2020;17(4):842–63. https://doi.org/10.20892/j.issn.2095-3941.2020.0005.
37. O'Doherty C, Keenan J, Horgan K, Murphy R, O'Sullivan F, Clynes M. Copper-induced non-monotonic dose response in Caco-2 cells. In Vitro Cell Dev Biol Anim. 2019;55:221–5. https://doi.org/10.1007/s11626-019-00333-8.
38. Ulukaya E, Acilan C, Yilmaz Y. Apoptosis: why and how does it occur in biology? Cell Biochem Funct. 2011;29(6):468–80. https://doi.org/10.1002/cbf.1774.
39. Silva MT. Secondary necrosis: the natural outcome of the complete apoptotic program. FEBS Lett. 2010;584(22):4491–9. https://doi.org/10.1016/j.febslet.2010.10.046.
40. Caca K, Feisthammel J, Klee K, Tannapfel A, Witzigmann H, Wittekind C, et al. Inactivation of the INK4a/ARF locus and p53 in sporadic extrahepatic bile duct cancers and bile tract cancer cell lines. Int J Cancer. 2002;97(4):481–8. https://doi.org/10.1002/ijc.1639.
41. Chen CC, Liao RY, Yeh FY, Lin YR, Wu TY, Pastor AE, et al. A simple and affordable method to create nonsense mutation clones of p53 for studying the premature termination codon readthrough activity of PTC124. Biomedicines. 2023;11(5):1310. https://doi.org/10.3390/biomedicines11051310.
42. Hiraki M, Hwang SY, Cao S, Ramadhar TR, Byun S, Yoon KW, Lee SW. Small-molecule reactivation of mutant p53 to wild-type-like p53 through the p53-Hsp40 regulatory axis. Chem Biol. 2015;22(9):1206–16.
43. Shimizu Y, Demetris AJ, Gollin SM, Storto PD, Bedford HM, Altarac S, Whiteside TL. Two new human cholangiocarcinoma cell lines and their cytogenetics and responses to growth factors, hormones, cytokines or immunologic effector cells. Int J Cancer. 1992;52(2):252–60.
44. Miyagiwa M, Ichida T, Tokiwa T, Sato J, Sasaki H. A new human cholangiocellular carcinoma cell line (HuCC-T1) producing carbohydrate antigen 19/9 in serum-free medium. In Vitro Cell Dev Biol. 1989;25(6):503–10. https://doi.org/10.1007/BF02623562.
45. Liu DP, Song H, Xu Y. A common gain of function of p53 cancer mutants in inducing genetic instability. Oncogene. 2010;29(7):949–56. https://doi.org/10.1038/onc.2009.376.
46. Lu X, Liu DP, Xu Y. The gain of function of p53 cancer mutant in promoting mammary tumorigenesis. Oncogene. 2013;32(23):2900–6. https://doi.org/10.1038/onc.2012.299.
47. Muller PA, Vousden KH. Mutant p53 in cancer: new functions and therapeutic opportunities. Cancer Cell. 2014;25(3):304–17. https://doi.org/10.1016/j.ccr.2014.01.021.
48. Willis A, Jung EJ, Wakefield T, Chen X. Mutant p53 exerts a dominant negative effect by preventing wild-type p53 from binding to the promoter of its target genes. Oncogene. 2004;23(13):2330–8. https://doi.org/10.1038/sj.onc.1207396.

49. Raggi C, Taddei ML, Rae C, Braconi C, Marra F. Metabolic reprogramming in cholangiocarcinoma. J Hepatol. 2022;77(3):849–64. https://doi.org/10.1016/j.jhep.2022.04.038.
50. Tanaka M, Kunita A, Yamagishi M, Katoh H, Ishikawa S, Yamamoto H, Ushiku T. KRAS mutation in intrahepatic cholangiocarcinoma: linkage with metastasis-free survival and reduced E-cadherin expression. Liver Int. 2022;42(10):2329–40.
51. Silva EL, Mesquita FP, Ramos INF, Gomes CBSMR, Moreira CDS, Ferreira VF, et al. Antitumoral effect of novel synthetic 8-hydroxy-2-((4-nitrophenyl)thio)naphthalene-1,4-dione (CNN16) via ROS-mediated DNA damage, apoptosis, and anti-migratory effect in colon cancer cell line. Toxicol Appl Pharmacol. 2022;456:116256. https://doi.org/10.1016/j.taap.2022.116256.
52. de Souza AS, Dias DS, Ribeiro RCB, Costa DCS, de Moraes MG, Pinho DR, et al. Novel naphthoquinone-1H-1,2,3-triazole hybrids: Design, synthesis and evaluation as inductors of ROS-mediated apoptosis in the MCF-7 cells. Bioorg Med Chem. 2024;102:117671. https://doi.org/10.1016/j.bmc.2024.117671.
53. Zhang Y, Luo YH, Piao XJ, Shen GN, Wang JR, Feng YC, et al. The design of 1,4-naphthoquinone derivatives and mechanisms underlying apoptosis induction through ROS-dependent MAPK/Akt/STAT3 pathways in human lung cancer cells. Bioorg Med Chem. 2019;27(8):1577–87. https://doi.org/10.1016/j.bmc.2019.03.002.
54. Pereyra CE, Dantas RF, Ferreira SB, Gomes LP, Silva-Jr FP. The diverse mechanisms and anticancer potential of naphthoquinones. Cancer Cell Int. 2019;19:207. https://doi.org/10.1186/s12935-019-0925-8.
55. Gharbaran R, Shi C, Onwumere O, Redenti S. Plumbagin induces cytotoxicity via loss of mitochondrial membrane potential and caspase activation in metastatic retinoblastoma. Anticancer Res. 2021;41(10):4725–32. https://doi.org/10.21873/anticanres.15287.
56. Chen PH, Lu HK, Renn TY, Chang TM, Lee CJ, Tsao YT, Chuang P, Liu JF. Plumbagin induces reactive oxygen species and endoplasmic reticulum stress-related cell apoptosis in human oral squamous cell carcinoma. Anticancer Res. 2024;44(3):1173–82. https://doi.org/10.21873/anticanres.16912.
57. Wellington KW. Understanding cancer and the anticancer activities of naphthoquinones—a review. RSC Adv. 2015;5(26):20309–38. https://doi.org/10.1039/C4RA13547D.
58. Thorn CF, Oshiro C, Marsh S, Hernandez-Boussard T, McLeod H, Klein TE, et al. Doxorubicin pathways: pharmacodynamics and adverse effects. Pharmacogenet Genomics. 2011;21(7):440–6. https://doi.org/10.1097/FPC.0b013e32833ffb56.
59. Liu J, Jiang G, Mao P, Zhang J, Zhang L, Liu L, et al. Down-regulation of gadd45a enhances chemosensitivity in melanoma. Sci Rep. 2018;8(1):4111. https://doi.org/10.1038/s41598-018-22484-6.
60. Jung H, Kim H, Kim Y, Weon J, Seo Y. A novel chemopreventive mechanism of selenomethionine: enhancement of ape1 enzyme activity via a gadd45a, pcna and ape1 protein complex that regulates p53-mediated base excision repair. Oncol Rep. 2013;30(4):1581–6. https://doi.org/10.3892/or.2013.2613.
61. Artykov AA, Belov DA, Shipunova VO, Trushina DB, Deyev SM, Dolgikh DA, et al. Chemotherapeutic agents sensitize resistant cancer cells to the DR5-specific variant DR5-B more efficiently than to TRAIL by modulating the surface expression of death and decoy receptors. Cancers. 2020;12(5):1129. https://doi.org/10.3390/cancers12051129.
62. Yang PY, Hu DN, Kao YH, Lin IC, Chou CY, Wu YC. Norcantharidin induces apoptosis in human prostate cancer cells through both intrinsic and extrinsic pathways. Pharmacol Rep. 2016;68(5):874–80. https://doi.org/10.1016/j.pharep.2016.04.010.
63. Dong Y, Yang G, Deng H, Chen W, An G. Gefitinib upregulates death receptor 5 expression to mediate rmhtrail-induced apoptosis in gefitinib-sensitive nsclc cell line. Oncotargets Ther. 2015;8:1603–10. https://doi.org/10.2147/ott.s73731.
64. Eum D, Byun J, Yoon C, Seo W, Park K, Lee J, et al. Triterpenoid pristimerin synergizes with taxol to induce cervical cancer cell death through reactive oxygen species-mediated mitochondrial dysfunction. Anticancer Drugs. 2011;22(8):763–73. https://doi.org/10.1097/CAD.0b013e328347181a.
65. Zheng H, Zhang Y, Zhan Y, Liu S, Lu J, Wen Q, et al. Expression of DR5 and c flip proteins as novel prognostic biomarkers for non-small cell lung cancer patients treated with surgical resection and chemotherapy. Oncol Rep. 2019;42(6):2363–70. https://doi.org/10.3892/or.2019.7355.
66. Surapally S, Jayaprakasam M, Verma RS. Curcumin augments therapeutic efficacy of TRAIL-based immunotoxins in leukemia. Pharmacol Rep. 2020;72(4):1032–46. https://doi.org/10.1007/s43440-020-00073-7.
67. Zappa F, Muniozguren NL, Conrad JE, Acosta-Alvear D. The integrated stress response engages a cell-autonomous, ligand-independent, DR5-driven apoptosis switch. Cell Death Dis. 2025;16(1):101.
68. Lam M, Lawrence DA, Ashkenazi A, Walter P. Confirming a critical role for death receptor 5 and caspase-8 in apoptosis induction by endoplasmic reticulum stress. Cell Death Differ. 2018;25(8):1530–1.
69. Roufayel R, Younes K, Al-Sabi A, Murshid N. BH3-only proteins Noxa and Puma are key regulators of induced apoptosis. Life (Basel, Switzerland). 2022;12(2):256. https://doi.org/10.3390/life12020256.
70. Okamoto K, Zaanan A, Kawakami H, Huang S, Sinicrope FA. Reversal of mutant KRAS-mediated apoptosis resistance by concurrent Noxa/Bik induction and Bcl-2/Bcl-xL antagonism in colon cancer cells. Mol Cancer Res. 2015;13(4):659–69.

Authors and Affiliations

Gizem Bulut[1,2] · Merve Kayis[3] · Dilan Gezer[4] · Zeliha Gokmen[4] · Zelal Adiguzel[3] · Chiara Raggi[5] · Engin Ulukaya[1,6]

✉ Engin Ulukaya
eulukaya@istinye.edu.tr

[1] Molecular Cancer Research Center (ISUMKAM), Istinye University, Istanbul, Turkey

[2] Department of Translational Medicine, Institute of Health Sciences, Acıbadem Mehmet Ali Aydınlar University, Istanbul, Turkey

[3] School of Medicine, KUTTAM, Koc University, Istanbul, Turkey

[4] Division of Organic Chemistry, Department of Chemistry, Faculty of Engineering, Istanbul University-Cerrahpasa, Istanbul, Turkey

[5] Department of Experimental and Clinical Medicine, University of Florence, Florence, Italy

[6] Department of Clinical Biochemistry, Faculty of Medicine, Istinye University, Istanbul, Turkey